NeuroImage: Clinical 24 (2019) 102091

Contents lists available at ScienceDirect

NeuroImage: Clinical

journal homepage: www.elsevier.com/locate/ynicl

Rasagiline, a monoamine oxidase B inhibitor, reduces *in vivo* [^{18}F]THK5351 uptake in progressive supranuclear palsy

Kok Pin Ng[a,b,c,1], Joseph Therriault[a,b,1], Min Su Kang[a,b], Hanne Struyfs[a,d], Tharick A Pascoal[a,b], Sulantha Mathotaarachchi[a,b], Monica Shin[a,b], Andrea L Benedet[a,b], Gassan Massarweh[e], Jean-Paul Soucy[e], Pedro Rosa-Neto[a,b,f,g], Serge Gauthier[a,b,*]

[a] Translational Neuroimaging Laboratory, The McGill University Research Centre for Studies in Aging, 6825 Boulevard LaSalle, Verdun, Montreal, QC H4H 1R3, Canada
[b] Alzheimer's Disease Research Unit, Douglas Hospital, McGill University, Montreal, Canada
[c] Department of Neurology, National Neuroscience Institute, Singapore
[d] Reference Center for Biological Markers of Dementia (BIODEM), University of Antwerp, Antwerp, Belgium
[e] McConnell Brain Imaging Centre, McGill University, 3801 University Street, Montreal, Québec H3A 2B4, Canada
[f] Montreal Neurological Institute, 3801 University Street, Montreal, Québec H3A 2B4, Canada
[g] Department of Neurology and Neurosurgery, McGill University, 3801 University Street, Montreal, Québec H3A 2B4, Canada

ARTICLE INFO

Keywords:
[^{18}F]THK5351 tau tracer
Monoamine oxidase-B
Rasagiline
Progressive Supranuclear Palsy
Positron emission tomography

ABSTRACT

Background: [^{18}F]THK5351 is a tau positron emission tomography tracer that has shown promise in quantifying tau distribution in tauopathies such as Alzheimer's disease (AD) and progressive supranuclear palsy (PSP). However, the interpretation of [^{18}F]THK5351 uptake has been shown to be confounded by high monoamine oxidase B (MAO-B) availability across the brain in AD.
Objectives: To test the hypothesis that the MAO-B inhibitor, rasagiline reduces [^{18}F]THK5351 uptake in PSP.
Methods: Six individuals (4: PSP; 2: cognitively unimpaired, CU) underwent [^{18}F]THK5351 and [^{18}F]AZD4694 to quantify baseline tau and amyloid deposition, respectively. Following a 10-day course of 1 mg rasagiline, all participants received a post-challenge [^{18}F]THK5351 scan. The baseline and post-rasagiline challenge standardized uptake value (SUV) were generated normalized for patient weight and injected radioactivity.
Results: The post-rasagiline regional SUV was reduced on average by 69–89% in PSP, and 53–81% in CU. The distributions of post-rasagiline [^{18}F]THK5351 SUV among PSP individuals were not consistent with the typical pattern of tau aggregates in PSP.
Conclusions: Similar to AD, the interpretation of [^{18}F]THK5351 uptake in PSP is likely confounded by off-target binding to MAO-B binding sites. [^{18}F]THK5351 is not sufficient in quantifying tau aggregates in PSP using the proposed rasagiline dosing regimen.

AD	Alzheimer's disease
PSP	Progressive Supranuclear Palsy
PET	Positron Emission Tomography
PHF	Paired Helical Filaments
NFT	Neurofibrillary Tangles
MAO-B	Monoamine Oxidase-B
MMSE	mini-mental state examination
PSPRS	progressive supranuclear palsy-rating scale
CU	cognitively unimpaired
SUV	Standardized Uptake Value
SUVR	Standardized Uptake Value Ratio.

1. Introduction

Tauopathies are neurodegenerative diseases characterized by the intracellular accumulation of hyperphosphorylated and abnormally aggregated tau proteins (Buée et al., 2000). These pathological tau proteins can be composed of 6 tau isoforms with either 3 repeats (3R) or 4 repeats (4R) of the microtubule binding domain. Progressive supranuclear palsy (PSP) is a 4R tauopathy characterized clinically by supranuclear gaze palsy, gait instability, parkinsonism and cognitive impairment (Boxer et al., 2017). Tau aggregates deposition in PSP has a distinct distribution affecting in particular the subthalamic nucleus,

* Corresponding author at: Alzheimer's Disease Research Unit, The McGill University Research Centre for Studies in A1geing, Montreal, c/o Douglas Hospital, McGill University, 6825 La Salle Blvd, H4H 1R3 Montreal, QC, Canada.
E-mail address: serge.gauthier@mcgill.ca (S. Gauthier).
[1] These authors contributed equally to this work.

https://doi.org/10.1016/j.nicl.2019.102091
Received 27 February 2019; Received in revised form 10 November 2019; Accepted 12 November 2019
Available online 13 November 2019

midbrain, and globus pallidus. Aggregates have a unique histopathological appearance of neurofibrillary tangles (NFT), with tufted astrocytes, coiled bodies and threads (Williams, 2006; Williams et al., 2007). However, given that tauopathies other than PSP such as corticobasal degeneration may manifest with a clinical presentation mimicking PSP, a definitive diagnosis of PSP is dependent on pathological confirmation from post-mortem examination. As such, the *in vivo* characterization of tau pathology using a tau positron emission tomography (PET) tracer capable of accurately diagnosing PSP would be highly useful as it could be a mean for selecting patients appropriate for a given therapy and to monitor treatment efficacy for PSP.

The advancement of tau tracer research has enabled the *in vivo* quantification of tau aggregates in tauopathies using PET imaging. [^{18}F]THK5351 is a quinoline-derivative tau imaging tracer with high affinity to paired helical filaments (PHF) present in NFT. In AD, which is characterized by hallmark pathologies of amyloid and NFT, retention of [^{18}F]THK5351 in the temporal lobes is able to distinguish AD from healthy controls (Harada et al., 2016), whereas in PSP, a recent study further demonstrates that [^{18}F]THK5351 uptake corresponds to tau lesions with selective binding to tufted astrocytes (Ishiki et al., 2017). In the same study, there is retention of [^{18}F]THK5351 in the globus pallidus and midbrain of PSP patients with the classic Richardson's syndrome, consistent with the typical neuropathological findings of classic Richardson's syndrome. Therefore, [^{18}F]THK5351 represents a promising tau PET tracer for the *in vivo* characterization of tau aggregates in both AD and PSP.

However, there are concerns regarding the specificity of [^{18}F]THK5351 for PHF given that [^{18}F]THK5351 is consistently observed to be retained in brain regions known to express negligible amounts of PHF in both AD and healthy individuals (Jang et al., 2018). In this regard, there is growing evidence demonstrating an off-target binding of [^{18}F]THK5351 to monoamine oxidase-B (MAO-B) binding sites in individuals with AD (Ng et al., 2017b), suggesting that the interpretation of [^{18}F]THK5351 PET scans as reflecting tau aggregation is confounded by the high MAO-B availability across the entire brain. Furthermore, a recent neuroimaging-pathological study also shows that [^{18}F]THK5351 PET uptake reflects MAO-B binding (Ishiki et al., 2018). Rasagiline is a selective MAO-B inhibitor (Lecht et al., 2007) and pharmacokinetic and pharmacodynamic studies of rasagiline show full saturation of MAO-B occupancy after a week of daily dosing, as measured by platelet MAO-B inhibition in healthy volunteers (Thébault et al., 2004). In addition, a [^{11}C]L-deprenyl PET study demonstrates *in vivo* full brain MAO-B occupancy after a 10 day course of daily 1 mg rasagiline (Freedman et al., 2005). Therefore, a rasagiline challenge using this dosing protocol prior to a [^{18}F]THK5351 PET scan constitutes a potential strategy to demonstrate the presence of off-target binding to MAO-B binding sites in PSP.

Here, in a competition study of probable PSP and cognitively unimpaired (CU) individuals undergoing baseline and post-rasagiline challenge [^{18}F]THK5351 PET scans, we test the hypotheses that a 10 day course of daily 1 mg rasagiline will reduce the uptake of [^{18}F]THK5351 in PSP, attributable to the off-target binding to MAO-B binding sites.

2. Methods

2.1. Study participants

In this study, we recruited patients with a clinical diagnosis of probable PSP based on the National Institute of Neurological Disorders and Stroke and the Society for PSP (NINDS-SPSP) criteria (Litvan et al., 1996) and CU controls not meeting the criteria of mild cognitive impairment (MCI) (Petersen, 2004) or dementia (McKhann et al., 2011) from the McGill University Research Center for Studies in Aging. All participants were screened to exclude any significant comorbid neurological, medical or psychiatric diseases and concomitant intake of MAO-inhibitors. All participants completed the mini-mental state examination (MMSE) (Folstein et al., 1975) to evaluate their global cognition. In addition, all PSP patients were examined by a neurologist to grade the severity of their PSP condition using the PSP rating scale (PSPRS) (Golbe and Ohman-Strickland, 2007). The PSPRS is a clinical scale that has been validated to measure disease progression and prognosis. It consists of 28 items grouped in 6 categories: daily activities, behavior, bulbar, ocular motor, limb motor and gait/midline signs. The PSPRS score ranges from 0 to 100 and a higher score indicates a poorer prognosis.

2.2. Ethics approval and consent to participate

The study has been approved by the McGill institutional review board and all participants signed an informed consent form prior to the study.

2.3. Scanning and dosing protocol

All participants underwent [^{18}F]THK5351 and [^{18}F]AZD4694 scans to quantify their baseline tau and amyloid loads respectively. All participants then received a daily oral dose of 1 mg rasagiline for a course of 10 days and their medication adherence was ensured *via* a daily phone call by a study coordinator. A post-challenge [^{18}F]THK5351 scan was conducted on the last day of the rasagiline dosing regimen. The last dose of 1 mg Rasagiline was given one hour before the second [^{18}F]THK5351 scan. There was an average of 14 days (SD = 0.54 days) between the baseline and post-rasagiline [^{18}F]THK5351 scans. All PET scans were performed on a Siemens High Resolution Research Tomograph (HRRT). The [^{18}F]THK5351 acquisition consisted of dynamic images acquired from immediately after the intravenous bolus injection to 70 min post-injection. The mean ± standard deviation (SD) injected radioactivity of [^{18}F]THK5351 was 6.9 ± 0.1 mCi for the baseline scan and 7.0 ± 0.1 mCi for the post-rasagiline scan. [^{18}F]AZD4694 acquisition consisted of dynamic images (6 × 5 min) acquired at 40–70 min after intravenous bolus injection of [^{18}F]AZD4694. The mean ± SD injected radioactivity of [^{18}F]AZD4694 was 6.7 ± 0.1 mCi. A six-minute transmission scan was performed following each PET scan for attenuation correction. Additionally, the images underwent correction for dead time and decay. All PET images were reconstructed using an Ordered Subsets Expectation Maximization (OSEM) algorithm (Alessio and Kinahan, 2006) which corrected for normalization, attenuation, randoms and scatter. In addition, inter-frame motion was corrected using the first frame as a reference. All patients also underwent a T1-weighted MP-RAGE anatomical MRI scan using a 3.0 T Siemens Sonata scanner for co-registration purposes and to evaluate for typical structural PSP features such as an abnormal midbrain to pons ratio (Massey et al., 2013).

2.4. Synthesis of [^{18}F]THK5351 and [^{18}F]AZD4694

[^{18}F]THK5351 was synthesized according to the previously published protocol (Harada et al., 2016). At the time of production, the average molar activity was 1702 ± 777 MBq/μmol for the baseline scan and 3256 ± 1554 MBq/μmol for the post-rasagiline dosing challenge scan. The average injected molar activity was 1135.9 ± 732.6 MBq/μmol for the baseline scan and 1605.8 ± 1454.1 MBq/μmol for the post-rasagiline dosing challenge scan (P = 0.49, not significant). The average injected mass dose was 14.94 ng/kg for the baseline scan and 12.62 ng/kg for the post-rasagiline dosing challenge scan (P = 0.70, not significant). [^{18}F]AZD4694 was synthesized using the previously published protocol (Cselényi et al., 2012), with an average molar activity of 3071 ± 518 MBq/μmol.

2.5. MRI and PET image processing

The T1-weighted MR images were processed using the CIVET image processing pipeline (Ad-Dab'bagh et al., 2006) and all PET images were processed using an established image processing pipeline previously reported (Ng et al., 2017a; Therriault et al., 2018). Briefly, individual PET and MRI images were co-registered using a rigid-body transformation based on 6 parameters. Then, the images were linearly co-registered and non-linearly spatially normalized to the standardized MNI152 template without modulation using an affine transformation from the PET/T1-MRI transformation and anatomical MRI registration.

Due to the presence of MAO-B in the reference region, full quantification of [^{18}F]THK5351 is not possible, as specific uptake in the reference region (in this case, the cerebellar grey matter) violates an assumption of the Simplified Reference Tissue Method (SRTM) (Salinas et al., 2015). Correspondingly, other reference tissue methods such as SUVR are also inappropriate. As such, we generated regional [^{18}F]THK5351 standardized uptake values (SUV) as a primary outcome measure. We measured the baseline and post-rasagiline [^{18}F]THK5351 SUV using tissue radioactivity data obtained 50–70 min after [^{18}F]THK5351 injection, normalized by patient body weight and injected radioactivity. SUV was measured in the substantia nigra, thalamus, subthalamic nucleus, internal globus pallidus, midbrain, dentate nucleus and cerebellar grey matter in PSP and CU participants. These regions were assessed using an atlas created for subjects with movement disorders (Xiao et al., 2017). The ROIs were subsequently applied to the dynamic PET frames to obtain the time–activity curve data. A basal ganglia meta-ROI was used to display time-activity curves, composed of the substantia nigra, subthalamic nucleus, internal & external globus pallidus, caudate and putamen. We then calculated the average percentage reduction of mean regional SUV in the post rasagiline scans. All participant's post-rasagiline [^{18}F]THK5351 SUV images were independently rated by two experts (JPS and PRN) in a blinded fashion as PSP-positive or PSP-negative. Cases were displayed on a system allowing visualization along the 3 standard axes, with the possibility of modifying the intensity settings of the colour scale. Interpretation was based on comparison to locally performed control cases: positive cases were those that, as subjectively assessed by the raters, showing increased and spatially different uptake when compared to controls in a manner consistent with published distributions of PSP pathology (Williams et al., 2007).

The [^{18}F]AZD4694 SUVR maps were processed using the cerebellar cortex as the reference region and each participant's [^{18}F]AZD4694 SUVR image was independently rated by two experts (JPS and PRN) as amyloid-positive or amyloid-negative. The midbrain to pons ratio was measured using the participant's sagittal T1-weighted MP-RAGE MRI image in native space. Based on previous reports, a midbrain to pons ratio of < 0.52 was considered supportive of a diagnosis of PSP, with a specificity of 100% and a sensitivity of 85.7% (Massey et al., 2013). Measurement of the midbrain to pons ratio was taken by placing elliptical regions of interest over the pons and midbrain in the midsaggital slice of the MRI in native space. Detailed description of this procedure as well as a visual representation of the methodology can be found in (Massey et al., 2013).

2.6. Statistical analysis

We performed the statistical analysis using the GraphPad Prism Version 7.0b (GraphPad Software, La Jolla, California, USA; www.graphpad.com). Paired *t*-test analyses were used to compare the baseline and post-rasagiline regional [^{18}F]THK5351 SUV.

3. Results

Six participants (4 probable PSP, and 2 CU) were recruited. Baseline demographics and clinical characteristics of the participants are summarized in Table 1.

Table 1
Baseline demographics and clinical characteristics.

	PT 1	PT 2	PT 3	PT 4	PT 5	PT 6
DIAGNOSIS	PSP	PSP	PSP	PSP	CU	CU
AGE (YEARS)	85	65	87	77	65	64
GENDER	F	M	M	M	F	M
MMSE	25	19	22	23	29	30
PSPRS	11	21	46	69	–	–
MIDBRAIN TO PONS RATIO	0.62	0.49	0.31	0.35	0.66	0.63

PT: participant; MMSE: mini-mental state examination; PSP: progressive supranuclear palsy; PSPRS: progressive supranuclear palsy-rating scale; CU: cognitively unimpaired.

3.1. Clinical profiles of the participants

Patient 1 was an 84 years old right-handed female who presented with progressive memory impairment, frequent falls and swallowing difficulties over four years. At the time of the PET scan, she had slowing of her eye movements, bradykinesia and postural instability. Her gait was slow with a cane and she had decreased spontaneous speech. Her MMSE was 24 and her PSPRS was 11 at the time of PET scanning. Her [^{18}F]AZD4694 scan was rated as amyloid positive (Fig. 1). The patient's midbrain to pons ratio was 0.62 (Fig. 2).

Patient 2 was a 64 years old right-handed male. His cognitive symptoms began three years prior to the study, when he started having language difficulties (such as mixing up words), executive dysfunction and frequent episodes of disorientation. Furthermore, he had difficulty performing activities of daily living and fell at least once a month due to gait difficulties. At the time of PET scanning, he presented with decreased voluntary upward saccades, neck rigidity, postural instability and apraxic gait with decreased right arm swing. His MMSE was 19 and his PSPRS was 21 at the time of PET scanning. His [^{18}F]AZD4694 scan was rated as amyloid negative (Fig. 1). The patient's midbrain to pons ratio was 0.49, consistent with a clinical diagnosis of PSP (Fig. 2).

Patient 3 was an 85 years old right-handed male and he first presented with a fall at age 83. His motor symptoms became progressively worse and the patient needed a cane and subsequently a walker as a walking aid. Clinical examination revealed decreased vertical saccades and supranuclear gaze palsy. At the time of the scanning sessions, he also had retropulsion and gait freezing while walking. His MMSE was 22 and his PSPRS was 46 at the time of PET scanning. His [^{18}F]AZD4694 scan was rated as amyloid negative (Fig. 1). The patient's midbrain to pons ratio was 0.31 and the sagittal section of his MRI demonstrated the typical “hummingbird sign” of midbrain atrophy, consistent with a clinical diagnosis of PSP (Fig. 2).

Patient 4 was a 72 years old right-handed male. He presented with gradually increasing limb stiffness and gait disturbance over the years, associated with cognitive impairment. Clinical examination revealed decreased vertical and horizontal saccades, dyskinesia, dysphagia, retropulsion, muscular rigidity and supranuclear gaze palsy. His MMSE was 23 and his PSPRS was 69 at the time of PET scanning. His [^{18}F]AZD4694 scan was rated as amyloid positive (Fig. 1). The patient's midbrain to pons ratio was 0.35, consistent with a clinical diagnosis of PSP (Fig. 2).

Patient 5 was a 65 years old right-handed female. Her MMSE was 29 at the time of PET scanning. Her [^{18}F]AZD4694 scan was rated as amyloid negative (Fig. 1). Patient 6 was a 64 years old right-handed male with subjective cognitive changes. His MMSE was 30 at the time of PET scanning. His [^{18}F]AZD4694 scan was rated as amyloid negative (Fig. 1). For both Patients 5 and 6, the clinical neurological examination and MRI study showed no changes to suggest PSP or AD.

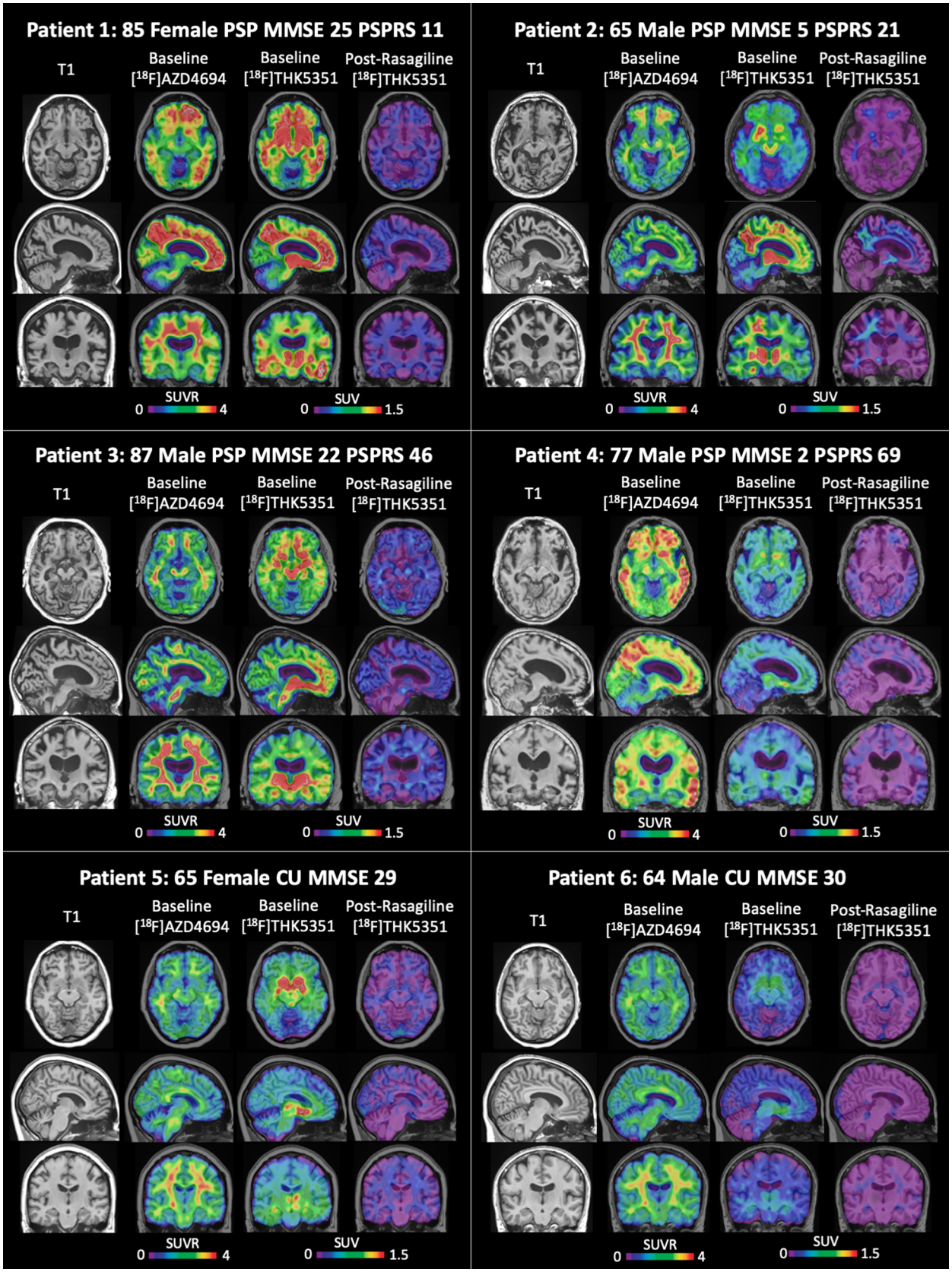

Fig. 1. Rasagiline reduces brain [^{18}F]THK5351 SUVs in progressive supranuclear palsy and cognitively unimpaired individuals. T1-weighted structural MRI, [^{18}F]AZD4694 standardized uptake value ratio (SUVR) and baseline and post-rasagiline [^{18}F]THK5351 Standardized Uptake Value (SUV) map in the six patients. MMSE Mini-Mental State Examination, PSPRS progressive supranuclear palsy rating scale; CU subjective cognitive changes; y.o years old.

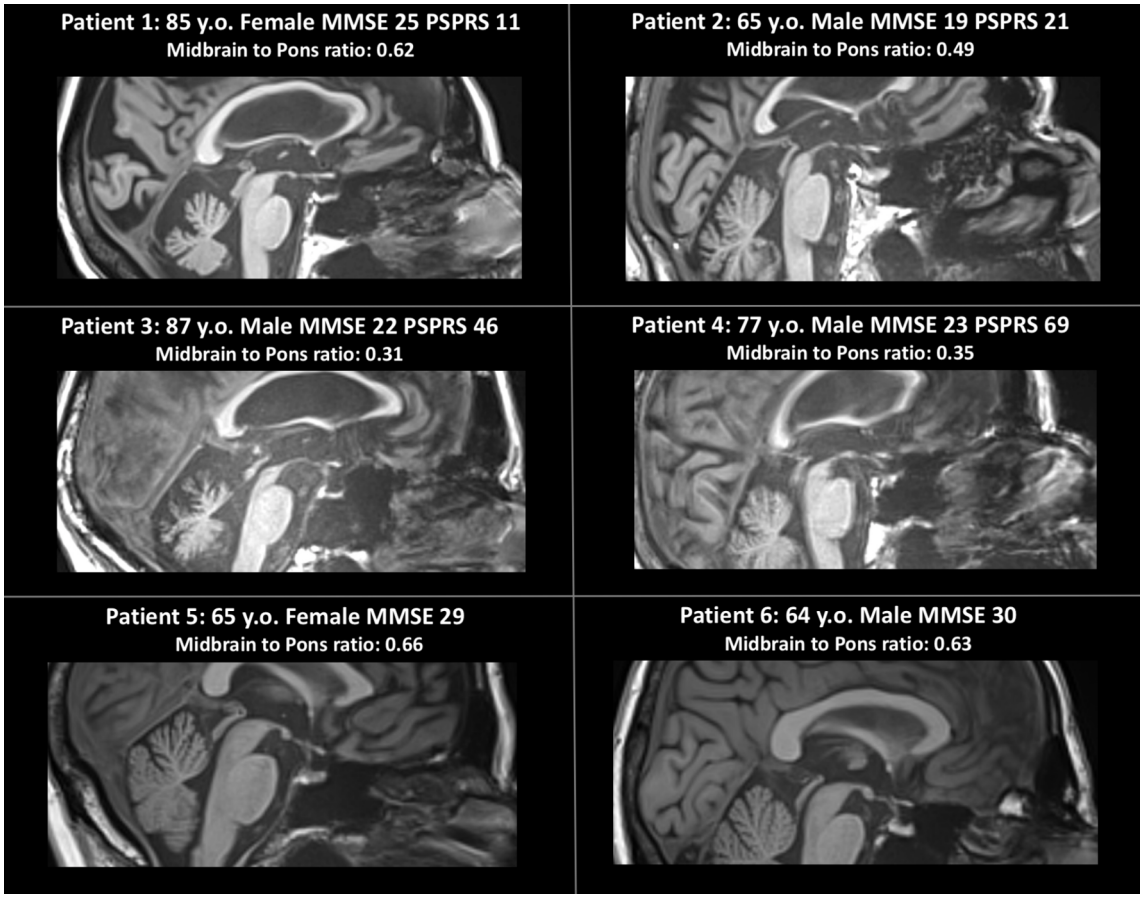

Fig. 2. Midbrain to pons ratio of the 6 study participants. Sagittal T1-weighted MRI showing the midbrain to pons ratio of the 6 patients. A midbrain to pons ratio < 0.52 is supportive of PSP. MMSE Mini-Mental State Examination, y.o years old.

3.2. Baseline regional [^{18}F]THK5351 uptake

Time–activity curves demonstrated that the radioactivity appeared quickly in the brain, with an SUV peak between 1 min and 3 min. [^{18}F]THK5351 cleared rapidly from the cerebellar grey matter, and more slowly in regions known to exhibit high concentrations of MAO-B such as the basal ganglia. Baseline regional [^{18}F]THK5351 time-activity curves for a representative subject are displayed in Fig. 3. Regional time-activity curves for all subjects are displayed in supplementary Fig. 1.

In PSP participants at baseline, the mean (standard deviation [SD]) [^{18}F]THK5351 SUV was highest in the internal globus pallidus (1.81 ± 0.73) followed by the subthalamic nucleus (1.48 ± 0.69), substantia nigra (1.41 ± 0.58), thalamus (1.34 ± 0.49), midbrain (1.17 ± 0.51) dentate nucleus (0.72 ± 0.38) and cerebellar grey matter (0.39 ± 0.13) (Table 2). In CU participants at baseline, the mean (SD) [^{18}F]THK5351 SUV was highest in the internal globus pallidus (0.98 ± 0.51) followed by the thalamus (0.72 ± 0.38), substantia nigra (0.71 ± 0.35), subthalamic nucleus (0.66 ± 0.35), midbrain (0.65 ± 0.33), dentate nucleus (0.42 ± 0.22) and cerebellar grey matter (0.25 ± 0.13).

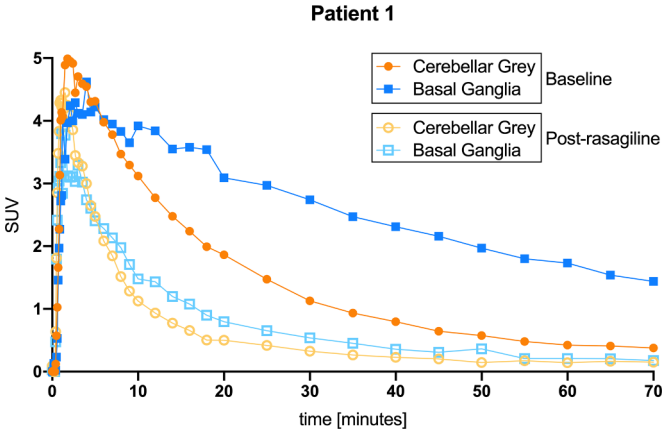

Fig. 3. Baseline and post-rasagiline regional time-activity curves for a representative subject. Regional standardized uptake value (SUV) time activity curves for baseline and post-rasagiline [^{18}F]THK5351 scans. Solid symbols represent baseline scans, while hollow symbols represent post-rasagiline scans. The basal ganglia is a meta-ROI composed of the substantia nigra, subthalamic nucleus, internal & external globus pallidus, caudate nucleus and putamen.

3.3. Post-rasagiline challenge regional [^{18}F]THK5351 uptake

In the post-rasagiline scans, time–activity curves demonstrated that the radioactivity appeared quickly in the brain, with an SUV peak between 1 min and 3 min. [^{18}F]THK5351 cleared more rapidly from the cerebellar grey matter as compared to the baseline scan. In post-rasagiline scans, [^{18}F]THK5351 also cleared more rapidly from MAO-B dense regions such as the basal ganglia as compared to baseline [^{18}F]THK5351 scans. There was no consistent difference in maximum [^{18}F]THK5351 SUV between pre and post-rasagiline in the basal ganglia or cerebellar grey matter. Post-rasagiline challenge regional [^{18}F]THK5351 time-activity curves for the same subject are displayed in Fig. 3. Regional time-activity curves for all subjects are displayed in supplementary Figure 1.

In the post-rasagiline scans of the PSP participants, the regional SUV

Table 2
Baseline and Post Rasagiline SUV.

	PT 1 PSP			PT 2 PSP			PT 3 PSP			PT 4 PSP			PT 5 CU			PT 6 CU		
BRAIN REGION	BL	PR	Δ%	BL	PR	Δ%	BL	PR	Δ%	BL	PR	Δ%	BL	PR	Δ%	BL	PR	Δ%
SUBSTANTIA NIGRA	1.47	0.22	85%	1.56	0.22	86%	2.01	0.31	85%	0.61	0.11	82%	0.95	0.18	81%	0.46	0.13	71%
THALAMUS	1.38	0.16	83%	1.47	0.12	91%	1.87	0.21	89%	0.67	0.09	87%	0.99	0.18	82%	0.45	0.1	77%
SUBTHALAMIC NUCLEUS	1.47	0.19	87%	1.69	0.20	88%	2.22	0.29	87%	0.55	0.1	82%	0.91	0.16	82%	0.41	0.12	70%
INTERNAL GLOBUS PALLIDUS	1.86	0.23	111%	2.05	0.45	78%	2.53	0.35	86%	0.79	0.11	86%	1.34	0.21	84%	0.61	0.14	77%
MIDBRAIN	1.14	0.16	67%	1.35	0.05	96%	1.71	0.19	88%	0.49	0.11	77%	0.88	0.16	82%	0.41	0.13	68%
DENTATE NUCLEUS	0.73	0.17	39%	0.56	0.07	88%	1.24	0.19	84%	0.36	0.12	66%	0.57	0.15	74%	0.26	0.11	57%
CEREBELLAR GREY MATTER	0.41	0.15	18%	0.31	0.06	80%	0.56	0.14	75%	0.27	0.11	59%	0.35	0.14	60%	0.16	0.09	43%

Table showing the regional baseline and post-rasagiline challenge Standardized Uptake Value (SUV) in each study participant. Substantial Nigra: $P = 0.0063$; Thalamus: $P = 0.0045$; Subthalamic Nucleus: $P = 0.011$; Globus Pallidus Internal: $P = 0.0046$; Midbrain: $P = 0.008$; Dentate Nucleus: $P = 0.0133$; Cerebellum Grey Matter: $P = 0.0049$. BL: baseline SUV; PR: postrasagiline challenge SUV; Δ%: percent change; PT: participant.

values were reduced on average by 69–89%, with the greatest average decline in the midbrain (88.8%) and thalamus (89.1%) (Table 2). In the post-rasagiline scans of the CU participants, the regional SUV values were reduced on average by 53–81%, with the greatest average decline in the thalamus (80.5%) and internal globus pallidus (81.6%). The post-rasagiline [^{18}F]THK5351 scans were rated as PSP negative in all participants. In the PSP participants, the distribution of [^{18}F]THK5351 was heterogeneous and not consistent with the typical distribution of tau aggregates deposition in PSP.

4. Discussion

In summary, we showed that *in vivo* quantification of tau aggregates in PSP using [^{18}F]THK5351 is likely confounded by off-target binding to MAO-B binding sites, consistent with our earlier findings in MCI and AD individuals (Ng et al., 2017b).

The high retention of [^{18}F]THK5351 in brain regions known to have negligible amounts of PHF has been attributed to off-target binding to MAO-B sites (Ishiki et al., 2018; Ng et al., 2017b). Supporting this hypothesis are results from a study we recently performed using a challenge experiment with the MAO-B inhibitor selegiline in mild cognitive impairment (MCI) and AD patients to test the effects of MAO-B inhibition on [^{18}F]THK5351 brain uptake. Following a single 10 mg oral dose of selegiline, the regional [^{18}F]THK5351 standardized uptake values (SUVs) decreased on average by 36.7–51.8%, with the greatest decline noted in the basal ganglia and thalamus, where the MAO-B concentrations are the highest (Ng et al., 2017b). In another PSP neuroimaging-pathological study, [^{18}F]THK5351 uptake in ante-mortem PET correlated with MAO-B, reactive astrocyte density, and tau pathology at post-mortem examination (Ishiki et al., 2018). In the subsequent *in vitro* autoradiography analysis, [^{18}F]THK5351 binding in areas of ante-mortem [^{18}F]THK5351 retention was completely blocked by lazabemide, a reversible selective MAO-B inhibitor. In the present study, we demonstrated that prolonged administration (10-day course of 1 mg per day) of rasagiline reduced [^{18}F]THK5351 uptake across brain regions on average by 69–89% in PSP and 53% to 81% in CU individuals. Therefore, our findings add to the growing list of reports that interpretation of [^{18}F]THK5351 uptake as seen with PET imaging as representative of tau aggregation is complicated by off-target binding to MAO-B binding sites.

Off-target binding occurs when there is displaceable binding to a receptor target other than the receptor target of interest. Given the presence of high MAO-B binding sites across the entire brain (Tong et al., 2013), it is likely that both the target (PHF) and off-target (MAO-B) binding sites for [^{18}F]THK5351 co-localise in similar brain regions in PSP. This leads to unreliable interpretation of [^{18}F]THK5351 PET images for differentiating fractions bound to PHF or MAO-B proteins in PSP as well as AD. In participants diagnosed with probable PSP, we demonstrated higher [^{18}F]THK5351 uptake in typical brain regions known to have higher tau aggregates in PSP on the baseline [^{18}F]THK5351 scans. However, when we utilized a prolonged rasagiline dosing protocol to block MAO-B binding sites, the residual [^{18}F]THK5351 uptake was heterogeneous and did not follow a typical regional distribution consistent with PSP. We found that [^{18}F]THK5351 uptake was displaced in both PSP-related regions including the subthalamic nucleus, substantia nigra and globus pallidus (Williams et al., 2007) and non PSP-related regions to varying levels. MAO-B expression level in the brain, for example in the globus pallidus, increases with age (Fowler et al., 1997). During the normal aging process, global MAO-B availability increases at the rate of nearly 9% per decade (Fowler et al., 1997). Furthermore, MAO-B protein levels are also reported to change in diseases such as AD (Schedin-Weiss et al., 2017) and Huntington's disease (Belendiuk et al., 1980). The variable expressions of MAO-B in the brain due to age and disease status suggest that a uniform dosing regimen using MAO-B inhibitors such as rasagiline may not be a satisfactory approach to resolve the issue of off-target binding of [^{18}F]THK5351 to MAO-B sites. Furthermore, the variable expression of MAO-B in the brain due to age and disease status affects the use of reference tissue methods for [^{18}F]THK5351 quantification.

MAO-B is a protein that is highly expressed in multiple brain regions, especially in histaminergic and serotonergic neurons (Saura et al., 1996). It is also present in the outer membrane of the astrocyte's mitochondria. [^{11}C]-L-deuteriodeprenyl is thought to bind to activated astrocytes and has been proposed to quantify astrocytosis in various neurodegenerative conditions such as AD (Carter et al., 2012; Santillo et al., 2011a). Patients with AD have been shown to express more MAO-B than controls matched for age (Santillo et al., 2011b), while post-mortem studies have demonstrated increased astrogliosis in patients with greater disease severity, which correlates significantly with tau pathology (Serrano-Pozo et al., 2011). Recent studies have further suggested that [^{18}F]THK5351 may prove useful as a neuroimaging biomarker of astrogliosis (Harada et al., 2017; Ishibashi et al., 2017). In our study, the higher [^{18}F]THK5351 SUVs in PSP at baseline suggests higher MAO-B availability in brain regions typical of PSP which may reflect locally increased astrogliosis in those areas. However, due to specific binding of [^{18}F]THK5351 to MAO-B in the cerebellar grey matter, further studies will be needed to determine whether [^{18}F]THK5351 can be used to assess astrogliosis with reference region methods.

Several methodological considerations limit the interpretation of the present study. Firstly, our study was conducted without measurements of the arterial input function. Hence, the interpretation of our results may be influenced by metabolic sources of variability or changes in cerebral blood flow. A second limitation of our study is the limited number of subjects as well as mixed pathologies, namely amyloid positivity in some of the older subjects (Jansen et al., 2015). While comorbidity of pathologies is common in neurodegenerative diseases (Gauthier et al., 2018; Schneider et al., 2007), a clinical misdiagnosis of PSP could result in a clinical-radiological mismatch where an image does not display a typical PSP pattern of uptake in a patient clinically

misdiagnosed with PSP. A third limitation is that the *in vivo* affinity of [^{18}F]THK5351 to MAO-B is unknown, but likely high, suggesting that the rasagiline challenge could potentially affect binding to both high and low affinity targets of [^{18}F]THK5351. Also, the ability of rasagiline to displace the binding of [^{18}F]THK5351 to tau is not known. Hence, it cannot be concluded that the percentage change in binding is exclusively due to reduction in MAO-B availability. Moreover, SUV has not yet been studied in the context of post-rasagiline [^{18}F]THK5351 PET scanning. Lastly, the use of SUV has limitations, including introducing variability of cerebral blood flow and tracer delivery, as well as other sources of physiological variability (Boellaard, 2009) which limit some of the interpretations of our study.

In summary, our study supports the concept that MAO-B is likely an off-target binding site of [^{18}F]THK5351 in PSP. Given the heterogeneous pattern of [^{18}F]THK5351 SUVs following the 10-day rasagiline challenge, [^{18}F]THK5351 is not sufficient for the quantification of tau aggregates in PSP using the proposed rasagiline dosing regimen.

Funding

This study is supported by the W & C Bentham Medical Research Fund and the Canadian Consortium for Neurodegeneration in Aging.

CRediT authorship contribution statement

Kok Pin Ng: Conceptualization, Methodology, Data curation, Formal analysis, Writing - original draft, Visualization, Project administration. **Joseph Therriault:** Conceptualization, Methodology, Data curation, Formal analysis, Writing - original draft, Visualization, Project administration. **Min Su Kang:** Methodology, Data curation, Writing - review & editing. **Hanne Struyfs:** Methodology, Data curation, Writing - review & editing. **Tharick A Pascoal:** Methodology, Data curation, Writing - review & editing. **Sulantha Mathotaarachchi:** Methodology, Data curation, Writing - review & editing. **Monica Shin:** Methodology, Data curation, Writing - review & editing. **Andrea L Benedet:** Methodology, Data curation, Writing - review & editing. **Gassan Massarweh:** Methodology, Data curation, Writing - review & editing. **Jean-Paul Soucy:** Methodology, Data curation, Writing - review & editing. **Pedro Rosa-Neto:** Conceptualization, Methodology, Data curation, Formal analysis, Writing - original draft, Visualization, Project administration, Supervision, Funding acquisition. **Serge Gauthier:** Conceptualization, Methodology, Data curation, Formal analysis, Writing - original draft, Visualization, Project administration, Supervision, Funding acquisition.

Declaration of Competing Interest

All authors have no disclosures

Supplementary materials

Supplementary material associated with this article can be found, in the online version, at doi:10.1016/j.nicl.2019.102091.

References

Ad-Dab'bagh, Y., Lyttelton, O., Muehlboeck, J.S., Lepage, C., Einarson, D., Mok, K., Ivanov, O., Vincent, R.D., Lerch, J., Fombonne, E., et al., 2006. The Civet image-processing environment: a fully automated comprehensive pipeline for anatomical neuroimaging research. In: Proceedings of the 12th Annual Meeting of the Organization for Human Brain Mapping, pp. 2266.

Alessio, A., Kinahan, P., 2006. PET image reconstruction. Nucl. Med. 1, 1–22. https://doi.org/10.1088/0031-9155/54/12/007.Iterative.

Belendiuk, K., Belendiuk, G.W., Freedman, D.X., 1980. Blood monoamine metabolism in Huntington's disease. Arch. Gen. Psychiatry 37, 325–332. https://doi.org/10.1001/archpsyc.1980.01780160095011.

Boellaard, R., 2009. Standards for PET image acquisition and quantitative data analysis. J. Nucl. Med. https://doi.org/10.2967/jnumed.108.057182.

Boxer, A.L., Yu, J.T., Golbe, L.I., Litvan, I., Lang, A.E., Höglinger, G.U., 2017. Advances in progressive supranuclear palsy: new diagnostic criteria, biomarkers, and therapeutic approaches. Lancet Neurol. 16, 552–563. https://doi.org/10.1016/S1474-4422(17)30157-6.

Buée, L., Bussière, T., Buée-Scherrer, V., Delacourte, A., Hof, P.R., 2000. Tau protein isoforms, phosphorylation and role in neurodegenerative disorders. Brain Res. Rev. 33, 95–130. https://doi.org/10.1016/S0165-0173(00)00019-9.

Carter, S.F., Scholl, M., Almkvist, O., Wall, A., Engler, H., Langstrom, B., Nordberg, A., 2012. Evidence for astrocytosis in prodromal Alzheimer disease provided by 11C-Deuterium-L-Deprenyl: a multitracer pet paradigm combining 11C-Pittsburgh Compound B and 18F-FDG. J. Nucl. Med. 53, 37–46. https://doi.org/10.2967/jnumed.110.087031.

Cselényi, Z., Jönhagen, M.E., Forsberg, A., Halldin, C., Julin, P., Schou, M., Johnström, P., Varnäs, K., Svensson, S., Farde, L., 2012. Clinical validation of 18F-AZD4694, an amyloid-β-specific PET radioligand. J. Nucl. Med. 53, 415–424. https://doi.org/10.2967/jnumed.111.094029.

Folstein, M.F., Folstein, S.E., McHugh, P.R., 1975. Mini-mental state". A practical method for grading the cognitive state of patients for the clinician. J. Psychiatr. Res. 12, 189–198. https://doi.org/10.1016/0022-3956(75)90026-6.

Fowler, J.S., Volkow, N.D., Wang, G.J., Logan, J., Pappas, N., Shea, C., MacGregor, R., 1997. Age-related increases in brain monoamine oxidase B in living healthy human subjects. Neurobiol. Aging 18, 431–435. https://doi.org/10.1016/S0197-4580(97)00037-7.

Freedman, N.M.T., Mishani, E., Krausz, Y., Weininger, J., Lester, H., Blaugrund, E., Ehrlich, D., Chisin, R., 2005. *In vivo* measurement of brain monoamine oxidase B occupancy by rasagiline, using (11)C-l-deprenyl and PET. J. Nucl. Med. 46, 1618–1624.

Gauthier, S., Zhang, H., Ng, K.P., Pascoal, T.A., Rosa-Neto, P., 2018. Impact of the biological definition of Alzheimer's disease using amyloid, tau and neurodegeneration (ATN): what about the role of vascular changes, inflammation, Lewy body pathology? Transl. Neurodegen. 7, 1–7. https://doi.org/10.1186/s40035-018-0117-9.

Golbe, L.I., Ohman-Strickland, P.A., 2007. A clinical rating scale for progressive supranuclear palsy. Brain 130, 1552–1565. https://doi.org/10.1093/brain/awm032.

Harada, Okamura, N., Furumoto, S., Furukawa, K., Ishiki, A., Tomita, N., Tago, T., Hiraoka, K., Watanuki, S., Shidahara, M., Miyake, M., Ishikawa, Y., Matsuda, R., Inami, A., Yoshikawa, T., Funaki, Y., Iwata, R., Tashiro, M., Yanai, K., Arai, H., Kudo, Y., 2016. 18F-THK5351: a novel pet radiotracer for imaging neurofibrillary pathology in Alzheimer's disease. J. Nucl. Med. 57, 208–214. https://doi.org/10.2967/jnumed.115.164848.

Harada, R., Ishiki, A., Kai, H., Sato, N., Furukawa, K., Furumoto, S., Tago, T., Tomita, N., Watanuki, S., Hiraoka, K., Ishikawa, Y., Funaki, Y., Nakamura, T., Yoshikawa, T., Iwata, R., Tashiro, M., Sasano, H., Kitamoto, T., Yanai, K., Arai, H., Kudo, Y., Okamura, N., 2017. Correlations of 18F-THK5351 pet with post-mortem burden of tau and astrogliosis in Alzheimer's disease. J. Nucl. Med. https://doi.org/10.2967/jnumed.117.197426.

Ishibashi, K., Kameyama, M., Tago, T., Toyohara, J., Ishii, K., 2017. Potential use of 18f-thk5351 PET to identify wallerian degeneration of the pyramidal tract caused by cerebral infarction. Clin. Nucl. Med. 42, e523–e524. https://doi.org/10.1097/rlu.0000000000001868.

Ishiki, A., Harada, R., Kai, H., Sato, N., Totsune, T., Tomita, N., Watanuki, S., Hiraoka, K., Ishikawa, Y., Funaki, Y., Iwata, R., Furumoto, S., Tashiro, M., Sasano, H., Kitamoto, T., Kudo, Y., Yanai, K., Furukawa, K., Okamura, N., Arai, H., 2018. Neuroimaging-pathological correlations of [18F]THK5351 PET in progressive supranuclear palsy. Acta Neuropathol. Commun. 6, 53. https://doi.org/10.1186/s40478-018-0556-7.

Ishiki, A., Harada, R., Okamura, N., Tomita, N., Rowe, C.C., Villemagne, V.L., Yanai, K., Kudo, Y., Arai, H., Furumoto, S., Tashiro, M., Furukawa, K., 2017. Tau imaging with [^{18} F]THK-5351 in progressive supranuclear palsy. Eur. J. Neurol. 24, 130–136. https://doi.org/10.1111/ene.13164.

Jang, Y.K., Lyoo, C.H., Park, S., Oh, S.J., Cho, H., Oh, M., Ryu, Y.H., Choi, J.Y., Rabinovici, G.D., Kim, H.J., Moon, S.H., Jang, H., Lee, J.S., Jagust, W.J., Na, D.L., Kim, J.S., Seo, S.W., 2018. Head to head comparison of [18F] AV-1451 and [18F] THK5351 for tau imaging in Alzheimer's disease and frontotemporal dementia. Eur. J. Nucl. Med. Mol. Imaging 45, 432–442. https://doi.org/10.1007/s00259-017-3876-0.

Jansen, W.J., Ossenkoppele, R., Knol, D.L., Tijms, B.M., Scheltens, P., Verhey, F.R.J., Visser, P.J., Aalten, P., Aarsland, D., Alcolea, D., Alexander, M., Almdahl, I.S., Arnold, S.E., Baldeiras, I., Barthel, H., Van Berckel, B.N.M., Bibeau, K., Blennow, K., Brooks, D.J., Van Buchem, M.A., Camus, V., Cavedo, E., Chen, K., Chetelat, G., Cohen, A.D., Drzezga, A., Engelborghs, S., Fagan, A.M., Fladby, T., Fleisher, A.S., Van Der Flier, W.M., Ford, L., Forster, S., Fortea, J., Foskett, N., Frederiksen, K.S., Freund-Levi, Y., Frisoni, G.B., Froelich, L., Gabryelewicz, T., Gill, K.D., Gkatzima, O., Gomez-Tortosa, E., Gordon, M.F., Grimmer, T., Hampel, H., Hausner, L., Hellwig, S., Herukka, S.K., Hildebrandt, H., Ishihara, L., Ivanoiu, A., Jagust, W.J., Johannsen, P., Kandimalla, R., Kapaki, E., Klimkowicz-Mrowiec, A., Klunk, W.E., Kohler, S., Koglin, N., Kornhuber, J., Kramberger, M.G., Van Laere, K., Landau, S.M., Lee, D.Y., De Leon, M., Lisetti, V., Lleo, A., Madsen, K., Maier, W., Marcusson, J., Mattsson, N., De Mendonca, A., Meulenbroek, O., Meyer, P.T., Mintun, M.A., Mok, V., Molinuevo, J.L., Mollergard, H.M., Morris, J.C., Mroczko, B., Van Der Mussele, S., Na, D.L., Newberg, A., Nordberg, A., Nordlund, A., Novak, G.P., Paraskevas, G.P., Parnetti, L., Perera, G., Peters, O., Popp, J., Prabhakar, S., Rabinovici, G.D., Ramakers, I.H.G.B., Rami, L., De Oliveira, C.R., Rinne, J.O., Rodrigue, K.M., Rodriguez-Rodriguez, E., Roe, C.M., Rot, U., Rowe, C.C., Ruther, E., Sabri, O., Sanchez-Juan, P., Santana, I., Sarazin, M., Schroder, J., Schutte, C., Seo, S.W., Soetewey, F., Soininen, H., Spiru, L., Struyfs, H., Teunissen, C.E., Tsolaki, M., Vandenberghe, R., Verbeek, M.M., Villemagne, V.L., Vos, S.J.B., Van Waalwijk Van Doorn, L.J.C., Waldemar, G., Wallin, A., Wallin, A.K., Wiltfang, J., Wolk, D.A., Zboch, M., Zetterberg, H., 2015. Prevalence of cerebral amyloid pathology in persons without dementia: a meta-analysis. JAMA 313,

1924–1938. https://doi.org/10.1001/jama.2015.4668.
Lecht, S., Haroutiunian, S., Hoffman, A., Lazarovici, P., 2007. Rasagiline – a novel MAO B inhibitor in Parkinson's disease therapy. Ther. Clin. Risk Manag. 3, 467–474.
Litvan, I., Agid, Y., Calne, D., Campbell, G., Dubois, B., Duvoisin, R.C., Goetz, C.G., Golbe, L.I., Grafman, J., Growdon, J.H., Hallett, M., Jankovic, J., Quinn, N.P., Tolosa, E., Zee, D.S., 1996. Clinical research criteria for the diagnosis of progressive supranuclear palsy (Steele-Richardson-Olszewski syndrome): report of the NINDS-SPSP international workshop. Neurology 47, 1–9. https://doi.org/10.1212/WNL.47.1.1.
Massey, L.A., Jager, H.R., Paviour, D.C., O'Sullivan, S.S., Ling, H., Williams, D.R., Kallis, C., Holton, J., Revesz, T., Burn, D.J., Yousry, T., Lees, A.J., Fox, N.C., Micallef, C., 2013. The midbrain to pons ratio: a simple and specific MRI sign of progressive supranuclear palsy. Neurology 80, 1856–1861. https://doi.org/10.1212/WNL.0b013e318292a2d2.
McKhann, G.M., Knopman, D.S., Chertkow, H., Hyman, B.T., Jack, C.R., Kawas, C.H., Klunk, W.E., Koroshetz, W.J., Manly, J.J., Mayeux, R., Mohs, R.C., Morris, J.C., Rossor, M.N., Scheltens, P., Carrillo, M.C., Thies, B., Weintraub, S., Phelps, C.H., 2011. The diagnosis of dementia due to Alzheimer's disease: recommendations from the National Institute on Aging-Alzheimer's Association workgroups on diagnostic guidelines for Alzheimer's disease. Alzheimer's Dement. 7, 263–269. https://doi.org/10.1016/j.jalz.2011.03.005.
Ng, K.P., Pascoal, T.A., Mathotaarachchi, S., Chung, C.O., Benedet, A.L., Shin, M., Kang, M.S., Li, X., Ba, M., Kandiah, N., Rosa-Neto, P., Gauthier, S., 2017a. Neuropsychiatric symptoms predict hypometabolism in preclinical Alzheimer disease. Neurology 88, 1814–1821. https://doi.org/10.1212/WNL.0000000000003916.
Ng, K.P., Pascoal, T.A., Mathotaarachchi, S., Therriault, J., Kang, M.S., Shin, M., Guiot, M.-.C., Guo, Q., Harada, R., Comley, R.A., Massarweh, G., Soucy, J.-.P., Okamura, N., Gauthier, S., Rosa-Neto, P., 2017b. Monoamine oxidase B inhibitor, selegiline, reduces 18F-THK5351 uptake in the human brain. Alzheimer's Res. Ther. 9, 25. https://doi.org/10.1186/s13195-017-0253-y.
Petersen, R.C., 2004. Mild cognitive impairment as a diagnostic entity. J. Int. Med. 183–194. https://doi.org/10.1111/j.1365-2796.2004.01388.x.
Salinas, C.A., Searle, G.E., Gunn, R.N., 2015. The simplified reference tissue model: model assumption violations and their impact on binding potential 304–311. 10.1038/jcbfm.2014.202.
Santillo, A.F., Gambini, J.P., Lannfelt, L., Långström, B., Ulla-Marja, L., Kilander, L., Engler, H., 2011a. *In vivo* imaging of astrocytosis in Alzheimer's disease: an 11C-L-deuteriodeprenyl and pib pet study. Eur. J. Nucl. Med. Mol. Imaging 38, 2202–2208. https://doi.org/10.1007/s00259-011-1895-9.
Santillo, A.F., Gambini, J.P., Lannfelt, L., Långström, B., Ulla-Marja, L., Kilander, L., Engler, H., 2011b. *In vivo* imaging of astrocytosis in Alzheimer's disease: an (11)C-L:-deuteriodeprenyl and PIB PET study. Eur. J. Nucl. Med. Mol. Imaging 1–32. https://doi.org/10.1007/s00259-011-1895-9.
Saura, J., Bleuel, Z., Ulrich, J., Mendelowitsch, A., Chen, K., Shih, J.C., Malherbe, P., Da Prada, M., Richards, J.G., 1996. Molecular neuroanatomy of human monoamine oxidases A and B revealed by quantitative enzyme radioautography and *in situ* hybridization histochemistry. Neuroscience 70, 755–774. https://doi.org/10.1016/S0306-4522(96)83013-2.
Schedin-Weiss, S., Inoue, M., Hromadkova, L., Teranishi, Y., Yamamoto, N.G., Wiehager, B., Bogdanovic, N., Winblad, B., Sandebring-Matton, A., Frykman, S., Tjernberg, L.O., 2017. Monoamine oxidase B is elevated in Alzheimer disease neurons, is associated with γ-secretase and regulates neuronal amyloid β-peptide levels. Alzheimer's Res. Ther. 9. https://doi.org/10.1186/s13195-017-0279-1.
Schneider, J.A., Arvanitakis, Z., Bang, W., Bennett, D.A., 2007. Mixed brain pathologies account for most dementia cases in community-dwelling older persons. Neurology 69, 2197–2204. https://doi.org/10.1212/01.wnl.0000271090.28148.24.
Serrano-Pozo, A., Mielke, M.L., Gómez-Isla, T., Betensky, R.A., Growdon, J.H., Frosch, M.P., Hyman, B.T., 2011. Reactive glia not only associates with plaques but also parallels tangles in Alzheimer's disease. Am. J. Pathol. 179, 1373–1384. https://doi.org/10.1016/j.ajpath.2011.05.047.
Thébault, J., Guillaume, M., Levy, R., 2004. Tolerability, safety, pharmacodynamics, and pharmacokinetics of rasagiline: a potent, selective, and irreversible monoamine oxidase type B inhibitor.: the journal of human ….
Therriault, J., Ng, K.P., Pascoal, T.A., Mathotaarachchi, S., Kang, M.S., Struyfs, H., Shin, M., Benedet, A.L., Walpola, I.C., Nair, V., Gauthier, S., Rosa-Neto, P., 2018. Anosognosia predicts default mode network hypometabolism and clinical progression to dementia. Neurology 90, e932–e939. https://doi.org/10.1212/WNL.0000000000005120.
Tong, J., Meyer, J.H., Furukawa, Y., Boileau, I., Chang, L.-.J., Wilson, A.A., Houle, S., Kish, S.J., 2013. Distribution of monoamine oxidase proteins in human brain: implications for brain imaging studies. Off. J. Int. Soc. Cereb. Blood Flow Metab. 33, 863–871. https://doi.org/10.1038/jcbfm.2013.19.
Williams, D.R., 2006. Tauopathies: classification and clinical update on neurodegenerative diseases associated with microtubule-associated protein tau. Int. Med. J. https://doi.org/10.1111/j.1445-5994.2006.01153.x.
Williams, D.R., Holton, J.L., Strand, C., Pittman, A., De Silva, R., Lees, A.J., Revesz, T., 2007. Pathological tau burden and distribution distinguishes progressive supranuclear palsy-parkinsonism from Richardson's syndrome. Brain 130, 1566–1576. https://doi.org/10.1093/brain/awm104.
Xiao, Y., Fonov, V., Chakravarty, M.M., Beriault, S., Al Subaie, F., Sadikot, A., Pike, G.B., Bertrand, G., Collins, D.L., 2017. A dataset of multi-contrast population-averaged brain MRI atlases of a Parkinson's disease cohort. Data Brief 12, 370–379. https://doi.org/10.1016/j.dib.2017.04.013.